Genome Biology

RESEARCH

Open Access

Dynamic and cell-type specific transcriptional reprogramming underlies the floral transition in the maize shoot apical meristem

Liang Dong[1,2†], Yonghao Sun[2,3†], Lu Kang[1,2], Zichao Li[1,2], Yameng Liang[4], Huangjun Sheng[1], Feng Tian[4], David Jackson[5] and Fang Yang[1,2*]

†Liang Dong and Yonghao Sun contributed equally to this work.

*Correspondence: yangf389@mail.sysu.edu.cn

[1] State Key Laboratory of Biocontrol, Guangdong Provincial Key Laboratory of Plant Stress Biology, School of Agriculture and Biotechnology, Sun Yat-Sen University, Shenzhen 518107, China
[2] National Key Laboratory of Crop Genetic Improvement, Huazhong Agricultural University, Wuhan 430070, China
[3] Hubei Hongshan Laboratory, Wuhan 430070, China
[4] National Maize Improvement Center of China, China Agricultural University, Beijing 100193, China
[5] Cold Spring Harbor Laboratory, Cold Spring Harbor, New York 11724, USA

Abstract

Background: The floral transition in maize represents a pivotal developmental switch that determines flowering time, environmental adaptation, and yield-related traits. However, the molecular mechanisms governing shoot apical meristem reprogramming and cell identity changes during this process remain poorly understood.

Results: By integrating time-course bulk RNA-seq, single-cell transcriptomics, chromatin accessibility, and transcription factor binding profiles, we construct a spatiotemporal molecular framework of the maize shoot apical meristem floral transition. Our analyses reveal global transcriptional reprogramming accompanied by pronounced cell type-specific regulation dynamics. At a global level, our transcriptional-level inference suggests that pathways associated with chromatin remodeling, environmental response, and reproductive development are sequentially activated. We further identify a *ZmMADS69-ZmRap2.7-ZMM4* regulatory module that fine-tunes the floral transition within the shoot apical meristem. At single-cell resolution, we find that the floral transition is not driven by a uniform transcriptional switch, but instead emerges from the coordinated action of spatially distinct shoot apical meristem domains. Through differential expression, trajectory, and co-expression module analyses, we further identify previously unrecognized roles for the inflorescence regulators *UNBRANCHED2* and *UNBRANCHED3* in promoting the floral transition, suggesting that they coordinate floral induction with subsequent inflorescence development.

Conclusions: Our study establishes a comprehensive spatiotemporal regulatory framework for the maize floral transition, providing mechanistic insights into shoot apical meristem reprogramming and offering a foundation for identifying new regulators to improve maize adaptation and yield.

Keywords: Maize, Shoot apical meristem, Floral transition, Flowering, Single-cell RNA sequencing

Background

Maize (*Zea mays* ssp. *mays*) was domesticated from its wild ancestor, teosinte (*Zea mays* ssp. *parviglumis*), in southwestern Mexico [1, 2]. Following domestication, maize experienced a rapid and extensive latitudinal expansion, now spanning more than 90 degrees from its center of origin [3]. This remarkable geographic spread was paralleled by the emergence of substantial natural variation in flowering time, facilitating adaptation to a wide range of photoperiodic and ecological conditions [4]. A critical developmental event underlying this adaptive plasticity is the transition of the shoot apical meristem (SAM) from the vegetative to the reproductive identity [5]. The timing of this transition in maize determines two major agronomic traits, leaf number and flowering time, thereby influencing plant architecture and crop yield.

In angiosperms, floral induction is orchestrated by a systemic mobile signal known as florigen, which integrates light cues and transmits them from the leaves to the SAMs [6, 7]. In *Arabidopsis*, FLOWERING LOCUS T (FT) has been identified as the important florigenic signal. FT is synthesized in leaves under inductive photoperiods, transported via the phloem, and forms a transcriptional activation complex with the bZIP factor FD in the SAM to initiate the floral transition [8–12]. In maize, *Zea CENTRORADIALIS 8* (*ZCN8*) is recognized as the functional ortholog of *Arabidopsis FT* and exhibits canonical florigenic properties [13, 14]. *ZCN8* is predominantly expressed in phloem cells in leaves and, when ectopically expressed at the shoot apex, is sufficient to induce precocious flowering [14]. Upstream regulation of *ZCN8* has been studied extensively, revealing a multilayered transcriptional network that integrates photoperiod signals [15]. Light signals are perceived by multiple phytochromes, including *ZmPHYB1*/*B2* and *ZmPHYC1/C2*, which transmit photoperiodic information to the circadian clock network [16–18]. This clock circuitry is composed of core oscillators and regulators such as homologs of *PSEUDORESPONSE REGULATOR* (*ZmPRR*), *LATE ELONGATED HYPOCOTYL* (*ZmLHY1/2*), *CIRCADIAN CLOCK ASSOCIATED1* (*ZmCCA1*), *TIMING OF CAB EXPRESSION1* (*ZmTOC1*), and *GIGANTEA* (*GI1a/1b*), collectively shaping daily rhythmic outputs [15, 19, 20]. Acting as key clock-output components, *GI1a/b* relay temporal information to downstream flowering regulators, including homologs of *CONSTANS*, *CONSTANS*-LIKE, *TOC1* (*ZmCCT9/10*) and *CONSTANS*-LIKE (*CONZ1*) [21–24], which in turn control the expression of the florigen *ZCN8* and thereby regulate the timing of floral transition in maize [14]. A limited number of downstream targets of *ZCN8* have been identified. For example, DELAYED FLOWERING 1 (DLF1), the maize ortholog of *FD*, interacts with ZCN8 in a conserved manner in the SAM to activate downstream floral signals [25–33]. Further, DLF1 directly activates the transcription of *ZMM4* and *ZmMADS67*, promoting the floral transition [34]. In addition to photoperiodic regulation, flowering time in maize is also controlled by an age-dependent pathway mediated by the sequential action of *miR156*, *SPL*, *miR172*, and *AP2* repressors. High levels of *miR156* repress *SPL* gene expression, whereas a gradual decline in *miR156* with age allows the accumulation of *SPL* factors, thereby promoting the acquisition of reproductive competence [35]. In maize, *ZmSPL13* and *ZmSPL29* have been identified as key *SPL* regulators of the floral transition, functioning in both leaves and the SAM. These *SPLs* directly activate *ZmMIR172C* and the florigen *ZCN8* in leaves, and promote the expression of floral identity genes *ZMM3* and *ZMM4* in the SAM [28]. *miR172* acts

downstream of *SPLs* to repress *AP2*-family transcription factors that function as floral repressors [35]. In maize, the *AP2* homolog *GLOSSY15* (*GL15*) acts as a negative regulator of flowering and directly regulates floral identity genes [36]. However, the broader transcriptional reprogramming landscape associated with the cell fate switch during maize floral induction remains largely undefined.

The floral transition in the SAM involves complex spatiotemporal coordination of gene expression and cellular reprogramming, leading to the specification of new organogenic domains and meristem identities. These processes rely on precise transcriptional regulation within distinct cell populations, yet conventional bulk transcriptomic approaches lack the resolution to expose such cellular heterogeneity. Recent advances in single-cell omics technologies, particularly single-cell RNA sequencing, have revolutionized plant developmental biology by revealing the molecular states/dynamics and cell fate transitions of diverse organs at the single-cell resolution [37–41]. In this study, we systematically investigated the SAM state dynamics associated with the floral transition in maize by coupling the transcriptomic features at bulk and single-cell RNA levels. By delineating molecular trajectories of cell differentiation and reconstructing the underlying regulatory networks, we provide a comprehensive view of the cellular and molecular changes during a critical developmental transition for flowering which determines maize adaptation and yield.

Results

The molecular features of the SAM during the floral transition

To dissect the molecular basis of SAM transition from vegetative to floral development, we profiled SAM transcriptomes at 14, 16, 18, 22, 26, and 28 days after sowing (DAS), spanning the whole process of floral transition (Fig. 1a). Principal component analysis (PCA) revealed strong consistency between biological replicates (Additional file 2: Table S1), and exposed a continuous trajectory which aligned with the developmental stages of SAM (Fig. 1b). Notably, samples from 26 and 28 DAS were distant from other time points (Fig. 1b), highlighting a major transcriptional reprogramming at the later stage of the floral transition. We then investigated the expression dynamics of several key genes associated with flowering time (*DLF1*, *ZMM4*, *ZMM15*, *ZAP1*, *ZmSPL13*, and *ZmSPL29*) and those associated with inflorescence development (*UNBRANCHED2* [*UB2*], *UNBRANCHED3* [*UB3*], *TASSELSHEATH4* [*TSH4*], and *RAMOSA* genes) (Additional file 1: Fig. S1a, b). The expression patterns of these genes across the transition stages aligned with their previously reported expression domains and functions [26–33]. These findings underscore the suitability of our data in delineating the floral transition.

To elucidate the gene expression dynamics during the floral transition, we performed k-means clustering on all differentially expressed genes (DEGs) by pairwise comparisons between six progressive tissues (Fig. 1c, Additional file 2: Table S2). This analysis identified seven gene clusters (RC1-RC7), each displaying unique expression patterns and enriched for distinct biological pathways (Fig. 1c, d). For example, genes in cluster RC1 showed strong expression at 14 DAS and were primarily associated with leaf morphogenesis, mitochondrial RNA modification, and phospholipid biosynthesis (Fig. 1c, d). These included the leaf primordia marker *DROOPING LEAF1 (DRL1)* and the leaf

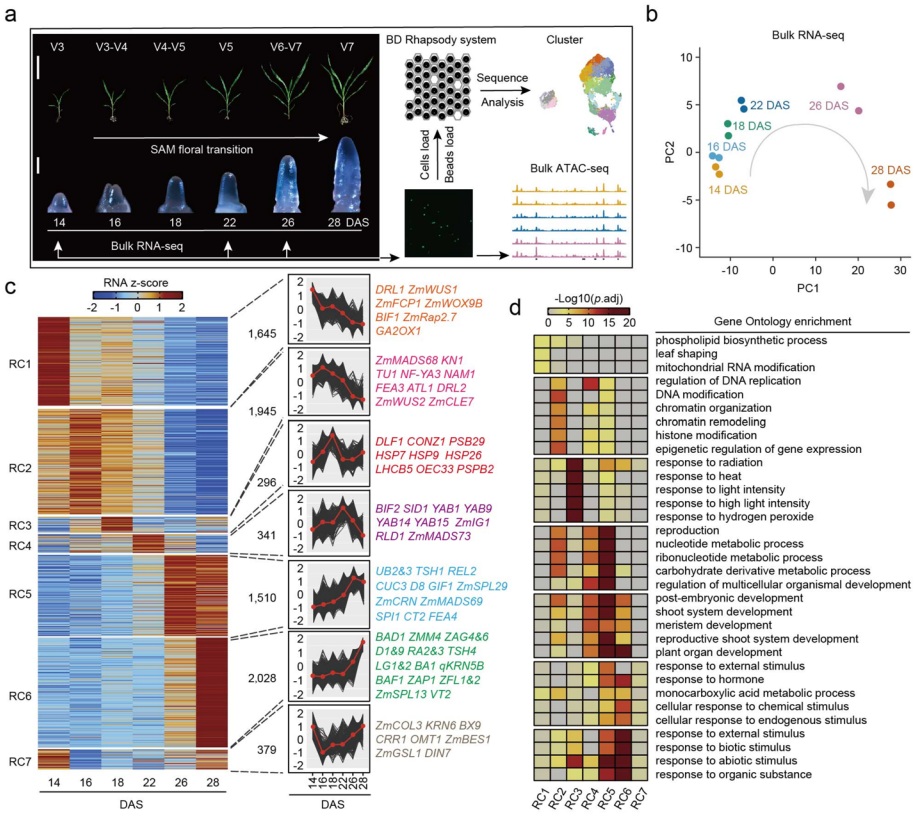

Fig. 1 Molecular dynamics of the maize SAM during the floral transition. **a** Representative SAM morphology at sequential developmental stages and overview of the experimental design. **b** Principal component analysis (PCA) of bulk RNA-seq data showing high reproducibility among replicates. Developmental trajectory from 14 to 28 DAS are indicated by an arrow. **c** Heatmap of differentially expressed genes (DEGs) grouped into seven RNA clusters (RC1-RC7) by *k*-means clustering across developmental stages. Line plots on the right depict the mean expression profiles of genes within each cluster, with representative regulators highlighted. **d** Heatmap showing top representative gene ontology (GO) terms enriched in each cluster

primordia-derived peptide gene *ZmFON2*-LIKE *CLE PROTEIN1* (*ZmFCP1*) which maintains meristem development [42, 43]. The high expression of flowering repressor *AP2* gene *ZmRap2.7* indicated that 14 DAS is in vegetative phase with active leaf formation. Genes in cluster RC2 displayed peak expression levels at 16 DAS and were enriched in processes related to chromatin remodelling as well as histone and DNA modifications (Fig. 1c, d), suggesting that epigenetic reprogramming plays a significant role in the maize SAM floral transition. This is in line with the epigenetic control of the flowering suppressor gene *FLOWERING LOCUS C* (*FLC*), whose repression mediated by strong histone modifications promotes the floral transition in *Arabidopsis* [44]. Meanwhile, the marked reduction in the flowering suppressor *ZmRap2.7* from 14 to 16 DAS (Additional file 1: Fig. S1a) indicated that the SAM at 16 DAS is likely undergoing the early floral transition. Subsequently, genes enriched at 18 DAS (RC3) were specifically associated with responses to environmental stimuli, such as light and temperature (Fig. 1d), suggesting that these genes may mediate environmental responses of SAM to induce the floral transition. At this stage (18 DAS) with the visible elongation of the SAM (Fig. 1a), the flowering-promoting factor *DLF1* reached peak expression (Additional file 1: Fig.

S1a, c), indicating that *DLF1* might accelerate the floral transition. By 22 DAS, genes (RC4) involved in reproductive shoot development were enriched, indicating that the floral transition was almost complete at this stage. In the subsequent stages, a large set of genes (RC5 and RC6) were robustly upregulated at 26 and 28 DAS (Fig. 1c). These genes were strongly associated with reproductive shoot development, nucleotide metabolism, and responses to both biotic and abiotic stimuli (Fig. 1d). Many key inflorescence regulators, such as *RAMOSA2* (*RA2*), *VANISHING TASSEL2* (*VT2*), and *UB3* (Fig. 1c, Additional file 1: Fig. S1b) [30, 31, 45], were included, highlighting their potential roles in early inflorescence meristem establishment. Taken together, these findings delineate the molecular dynamics of the maize SAM during the floral transition. On the basis of these molecular signatures, we propose that the SAM can be broadly divided into three developmental phases: a vegetative phase before 14 DAS, a transitional phase spanning approximately 16–22 DAS, and a post-transition phase commencing on or before 26 DAS.

Dynamic transcription factor regulation uncovers a floral transition module

Transcription factors (TFs), such as *ZmRap2.7*, *DLF1* and *ZmMADS69* play critical roles during the floral transition in maize [14, 26, 46, 47]. To expose the potential TF classes related to the distinct expression patterns during the floral transition, we first captured genome-wide open chromatin regions (OCRs) by performing ATAC-seq on SAM samples at 14, 22, and 26 DAS, which represent the three major developmental phases of the SAM (Additional file 2: Table S1 and S3). All three time points yielded high-quality data (Additional file 1: Fig. S2a-d). To provide a comprehensive catalogue of accessible chromatin regions, we merged OCRs from the three stages and used this unified set to perform TF motif enrichment analyses on OCRs located in the promoters of genes from different expression clusters (RC1-RC7). This analysis focused on identifying cluster-associated regulatory motifs underlying distinct RNA expression programs, rather than stage-specific chromatin accessibility dynamics, as time-resolved ATAC-seq data across additional stages were limited. The binding motifs of six TF families, TCP, SBP, ERF, ARF, MYB-related, and C2H2, were enriched across nearly all gene clusters (Fig. 2a), suggesting that these families likely act as general regulators of DEGs during the floral transition. Notably, some TF binding motifs also exhibited preferential or even specific enrichment in certain gene clusters. For example, AP2 and ARR-B binding motifs were exclusively enriched in RC1, which was active at the early phase (Fig. 2a). Consistent with this motif enrichment, 11 *AP2* genes and two *ARR* genes were preferentially expressed at this early stage (Additional file 1: Fig. S3a, b, Additional file 2: Table S4). Importantly, several members of these families, including the *AP2* genes *ZmRap2.7* and *GL15*, as well as the *ARR* gene *ARR11*, function as repressors of flowering [48]. These observations suggest that AP2- and ARR-mediated transcriptional programs may contribute to maintaining a repressive state during the early phase of floral transition. The motifs of LBD, DOF, and G2-like TFs were specifically enriched in RC2, RC3, or RC4 (Fig. 2a), which correspond to the ongoing floral transition during 16–22 DAS, implying potential for these TF families in floral transition. Consistent with this motif enrichment, two *LBD*, four *DOF*, and seven *G2*-like genes were preferentially expressed during this period (Additional file 1: Fig. S3c-e, Additional file 2: Table S4). Notably, a substantial

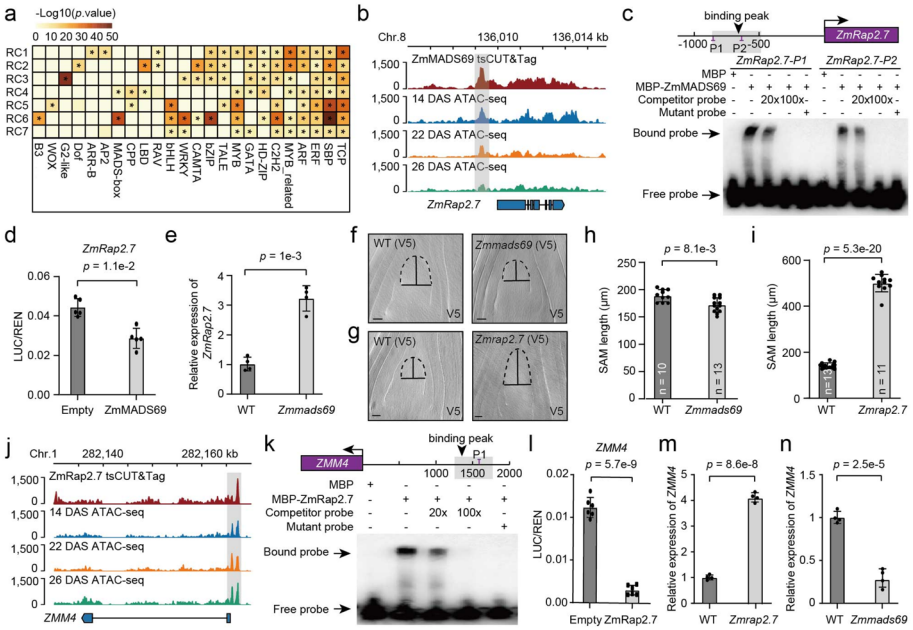

Fig. 2 Dynamic transcription factor regulation uncovers a floral transition module. **a** HOMER DNA-motif enrichment in OCRs located in promoters of genes from different expression clusters (RC1-RC7). Asterisks indicate significant enrichment ($p < 1e\text{-}5$). **b** ZmMADS69 binding sites detected in OCRs of *ZmRap2.7*. **c** EMSA revealed that recombinant MBP-ZmMADS69 could directly bind to the P1 and P2 regions of *ZmRap2.7*, which are located within the ZmMADS69 binding peak. The EMSA assays were performed with two independent biological replicates. **d** Dual-luciferase reporter assay showing that ZmMADS69 represses *ZmRap2.7* expression. **e** RT-qPCR showing reduced *ZmRap2.7* expression in the *Zmmads69* mutant relative to WT. **f, g** Representative images of SAMs from WT, *Zmmads69* (**f**), and *Zmrap2.7* (**g**) at V5 stages. Black lines indicate SAM regions for length and diameter measurements. Scale bars, 50 μm. **h**, **i** Quantification of SAM length in WT, *Zmmads69* (**h**), and *Zmrap2.7* (**i**) plants at V5 stages. **j** ZmRap2.7 binding sites detected in OCRs of *ZMM4*. **k** EMSA revealed that recombinant MBP-ZmRap2.7 could directly bind to the P1 regions located within the ZmRap2.7 binding peak of *ZMM4*. The EMSA assays were performed with two independent biological replicates. **l** Dual-luciferase reporter assay showing that ZmRap2.7 represses *ZMM4* expression. **m**, **n** RT-qPCR showing increased *ZMM4* expression in *Zmrap2.7* mutant (**l**) and reduced expression in *Zmmads69* mutant (**m**). All statistical analyses were performed using two-tailed *t*-tests

number of genes from these TF families were further enriched at later stages (26 and 28 DAS) (Additional file 1: Fig. S3c-e, Additional file 2: Table S4), suggesting that they may also contribute to the transition at subsequent developmental stages. At later stages, the gene cluster RC6, which shows peak expression at ~28 DAS, was enriched for MADS-box motifs (Fig. 2a). Consistent with this enrichment, 19 *MADS-box* genes were highly expressed at these later stages, including several well-established flowering promoters such as *ZMM4*, *ZmMADS67*, *ZmMADS69*, *ZMM3*, and *ZAP1* (Additional file 1: Fig. S3f, Additional file 2: Table S4). This pattern is consistent with the activation of floral identity and organ identity programs during the late phase of floral transition. Together, these motif enrichment results highlight the stage-specific TF families that coordinate the transcriptional regulation of SAM during the floral transition.

These stage-resolved motif and expression patterns suggested that distinct TF families are deployed in a temporally ordered manner during the floral transition, raising the possibility of direct regulatory interactions between early- and late-acting factors. As a representative example, the *AP2* flowering repressor *ZmRap2.7* reached peak expression at 14 DAS [46], consistent with AP2 motif enrichment in RC1 (Fig. S1a, Fig. 2a), whereas

the MADS-box flowering promoters *ZmMADS69* and *ZMM4* were preferentially expressed at 22–28 DAS [27, 47], when MADS-box motifs were enriched. The largely opposing expression trajectories between *ZmRap2.7* and *ZmMADS69*/*ZMM4* (Fig. S1a) prompted us to investigate whether these TFs form a regulatory module controlling floral transition. We first performed tsCUT&Tag sequencing and identified 3,647 and 7,083 binding peaks for *ZmMADS69* and *ZmRap2.7*, respectively (Additional file 2: Table S5 and S6). Both TFs showed strong TSS enrichment and high FRiP scores (fraction of reads in peaks), with highly correlated biological replicates (Additional file 1: Fig. S4a-c, Additional file 2: Table S1), indicating the high quality of the data. More than half (66%, and 60%, respectively) of the peaks were located in the promoter regions (Additional file 1: Fig. S4d) and thousands of target genes (3,118 and 5,539, respectively) were identified. Notably, 2,330 genes (75% or 42%, respectively) were co-bound by both TFs, suggesting that they may antagonistically regulate a shared set of downstream genes (Additional file 1: Fig. S4e). Interestingly, we found a ZmMADS69 binding peak in the *ZmRap2.7* promoter (Fig. 2b). We used electrophoretic mobility shift (EMSA) and dual-luciferase reporter assays to show that ZmMADS69 directly binds the "CArG" sites within the peak and represses *ZmRap2.7* expression (Fig. 2c, d, Additional file 1: Fig. S5a). Mutant analysis supported these molecular interactions. For example, *ZmRap2.7* was upregulated in the SAM of *Zmmads69* mutant (Fig. 2e) and V5 stage SAMs were significantly shorter in *Zmmads69* mutants and a significantly taller in *Zmrap2.7* mutants (Fig. 2f-i), demonstrating their antagonistic roles in the SAM floral transition. Furthermore, we also found a ZmRap2.7 binding peak in the promoter of another floral activator, *ZMM4* (Fig. 2j). EMSA, dual-luciferase reporter, and mutant expression assays demonstrated that ZmRap2.7 directly binds the "GCC-box" sites within this peak, and represses *ZMM4* expression in the SAM (Fig. 2k-n, Additional file 1: Fig. S5b). Collectively, these results support a regulatory module in which *ZmMADS69* directly represses *ZmRap2.7*, which subsequently directly represses *ZMM4*, thereby coordinating the floral transition in maize.

Single-cell RNA sequencing uncovers cell types associated with the floral transition

To further investigate the cell fate transition and the underlying molecular changes during the floral transition, we performed scRNA-seq analysis on SAMs containing the two youngest leaf primordia (SAM + P1 and P2) at 14, 22, and 26 DAS, representing three distinct developmental phases of the SAM transition (Fig. 1a). After quality control and batch-effect correction, we obtained 5,746–5,988 cells per sample, with median unique molecular identifier (UMI) counts of 6,343–8,538 and median expressed genes of 3,521–4,344 (Additional file 1: Fig. S6, Additional file 2: Table S1). In total, 17,563 merged cells were classified into 18 cell clusters using Seurat [49], which were further grouped into 8 major cell populations based on marker gene expression (Fig. 3a, Additional file 2: Table. S7). The vascular cell (VC) population, comprising clusters 1, 11, 17, and 18, was characterized by the general vascular markers *UMC1283* and *C2C2-DOF TRANSCRIPTION FACTOR 11* (*DOF11*), the phloem marker *ALTERED PHLOEM DEVELOPMENT1* (*ZmAPL1*), and the xylem marker *TARGET OF MONOPTEROS5* (*ZmTMO5*) (Fig. 3b, c, Additional file 1: Fig. S7a). The epidermal cell (EC) population (clusters 8, 10, 12, and 16) showed strong expression of epidermal markers *LIPID TRANSFER PROTEIN 2*

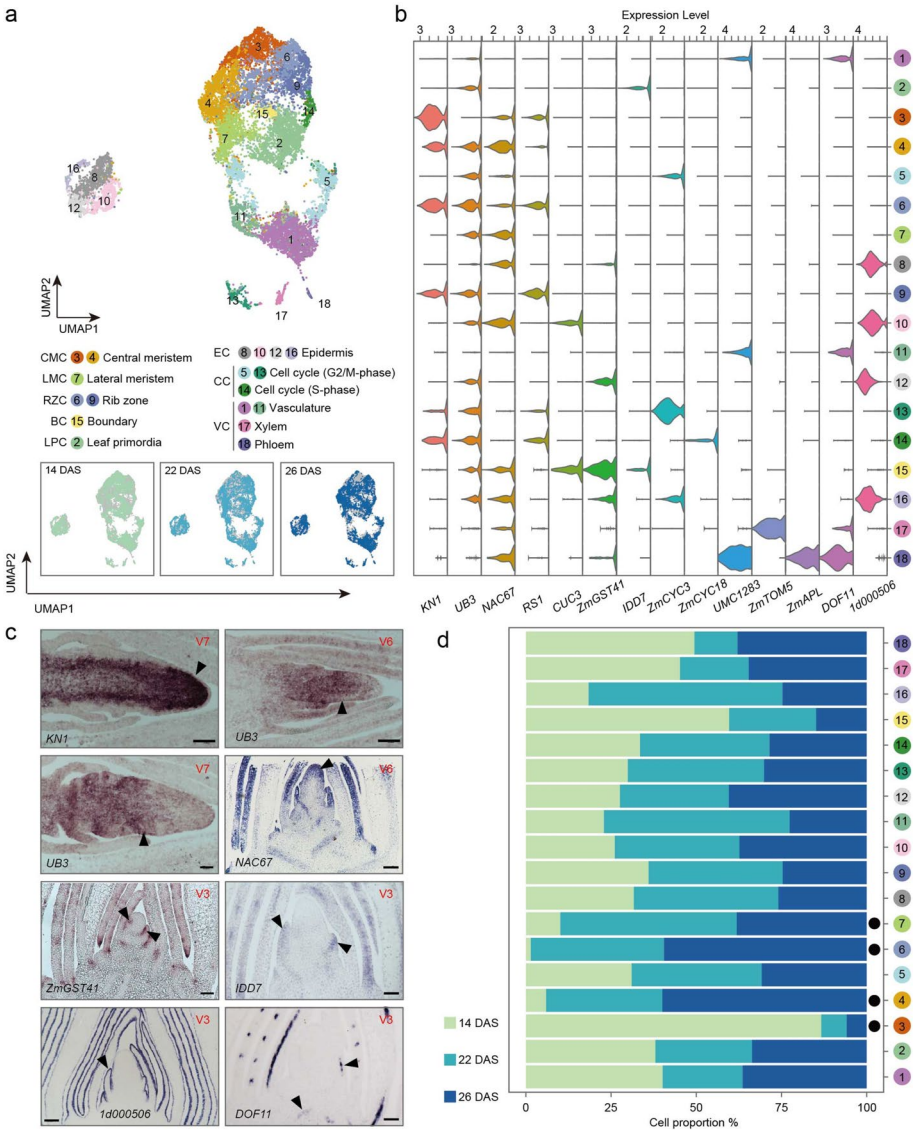

Fig. 3 scRNA-seq defines SAM cell-type identities and reveals cellular heterogeneity during the floral transition. **a** UMAP visualization of 18 clusters, with each dot representing a single cell and colors indicating different clusters. Lower panels indicate cell distributions of three stage cells, shown by colors. **b** Violin plots showing expression patterns of marker genes used for cell-type annotation. **c** RNA in situ hybridization validating selected marker genes. Scale bars, 100 μm. **d** Cell proportions of the 18 cluster at 14, 22, and 26 DAS, with stage-enriched clusters highlighted by black dots

(*LTP2*) and *Zm00001d000506* (Fig. 3b, c, Additional file 1: Fig. S7a). The leaf primordia cell (LPC) population (cluster 2) was identified by expression of leaf primordium markers *DROOPING LEAF 1* (*DRL1*) and *INDETERMINATE DOMAIN7* (*IDD7*), while the boundary cell (BC) population (cluster 15) expressed boundary-specific markers including *CUP-SHAPED COTYLEDON 3* (*ZmCUC3*) and *ZmGLUTATHIONE TRANSFERASE 41* (*ZmGST41*) (Fig. 3b, c, Additional file 1: Fig. S7a).

We next focused on the meristem-associated cell types. The meristem marker *KNOTTED1* (*KN1*) was broadly expressed throughout the SAM corpus excluding from the epidermis and lateral domains, and was enriched in clusters 3, 4, 6, and 9 (Fig. 3b, c,

Additional file 1: Fig. S7b). Among these clusters, clusters 6 and 9 also showed enrichment of *UB3* and *ROUGH SHEATH1* (*RS1*), two genes expressed at the SAM base (Fig. 3b, c, Additional file 1: Fig. S7a, b) [30, 50], and were thus designated as rib zone cells (RZC). *NAC67* was enriched in clusters 3 and 4 but not in clusters 6 and 9 (Fig. 3b, Additional file 1: Fig. S7b), and RNA in situ hybridization showed that *NAC67* marked the upper SAM (Fig. 3c). Accordingly, clusters 3 and 4 represented the upper region of the SAM and were defined as central meristem cells (CMC) (Fig. 3a). By contrast, cluster 7, enriched for *UB3* and *NAC67* but lacking *KN1* expression (Fig. 3b), was identified as lateral meristem cells (LMC), consistent with RNA in situ hybridization results showing that *UB3* and *NAC67* also mark the SAM lateral zone (Fig. 3c). The accuracy of our cell identity annotations was validated through marker-based module scoring using established maize shoot apex markers (Additional file 1: Fig. S8) [39].

Our preliminary analysis of cell proportions across developmental stages revealed stage-enriched clusters 3, 4, 6, and 7 attracting our attention (Fig. 3d). In the CMC population, cluster 3 was predominantly derived from vegetative SAM at 14 DAS, whereas cluster 4 mainly was originated from SAM undergoing floral induction at 22 and 26 DAS (Fig. 3d). This indicates that central meristem undergoes significant changes at the transcription state during the transition. Cluster 7 (LMC) was largely composed of cells from the induced SAM (Fig. 3d), suggesting that lateral meristems emerge during the early floral transition. The presence of another induced-SAM enriched cluster 6 (RZ) after 22 DAS was in line with the rapid expansion of rib zone during transition. As supports, some known flowering repressors (*ZmPRR37a*, *ZmLHY1, CONSTANS*-like *3* [*ZmCOL3*], *ZmCCA1*, *GA2ox1*) were enriched in the early-stage cluster 3, whereas some flowering promoters (*ZmSPL13*, *ZmMADS67*, *ZMM4*, *ZmGI1a*, *ZmGIb*, *UB2*, *UB3*) were preferentially expressed in clusters 4, 6, and 7 (Additional file 1: Fig. S9). Together, the stage-enriched expression patterns imply that central meristem, lateral meristem and rib zone are closely related to the floral induction process.

To be honest, changes in cell proportions across developmental stages and differences in transcriptional activity for each cell population should be considered with the absence of independent biological replicates. To mitigate this limitation, we performed cross-validation analyses using pseudobulk comparisons with independent bulk RNA-seq datasets and also with published maize single-cell datasets [39, 41, 51–60], which showed high concordance (Additional file 1: Fig. S10 and S11). Nevertheless, future studies incorporating biological replication and spatial transcriptomic approaches will be useful to validate the molecular dynamics observed in this study.

Spatiotemporal transcriptional dynamics across distinct meristem domains during the floral transition

To investigate the molecular changes associated with cell fate determination during the floral transition, we identified DEGs between adjacent developmental stages for each cell type. We focused on clusters CMC, LMC, RZ, LPC, and VC, which represent core cell populations sustaining the floral transition. Across these comparisons, we detected distinct transcriptional signatures ranging from 32 to 967 DEGs per comparison (Additional file 1: Fig. S12a, Additional file 2: Table S8 and S9), identifying a total of 1,817 and 1,815 DEGs during the early and late transition stages, respectively. Gene ontology

analysis revealed that temperature response pathway was strongly enriched in DEGs across most cell types (CMC, RZC, LPC, and VC) (Fig. 4a, c), implying that temperature plays a critical role in the maize floral transition. Concurrently, we observed significant enrichment for pathways involving organic, inorganic and metabolic substances (such as hormones, ROS). Notably, genes associated with chromatin organization processes were highly enriched in the CMC, RZC, and VC clusters, which had the most striking transcriptional dynamics (Fig. 4a), implying that the epigenetic states in these cells might undergo significant changes and be associated with the transcriptional changes.

Most of the DEGs were largely cell-type specific (Additional file 1: Fig. S12b), suggesting that the maize SAM responds to induction signals through spatially distinct gene sets in distinct cell domains. For example, *DLF1*, a key mediator of florigen signalling [26, 34], was specifically upregulated in LPC and RZC (Fig. 4a, e), suggesting these

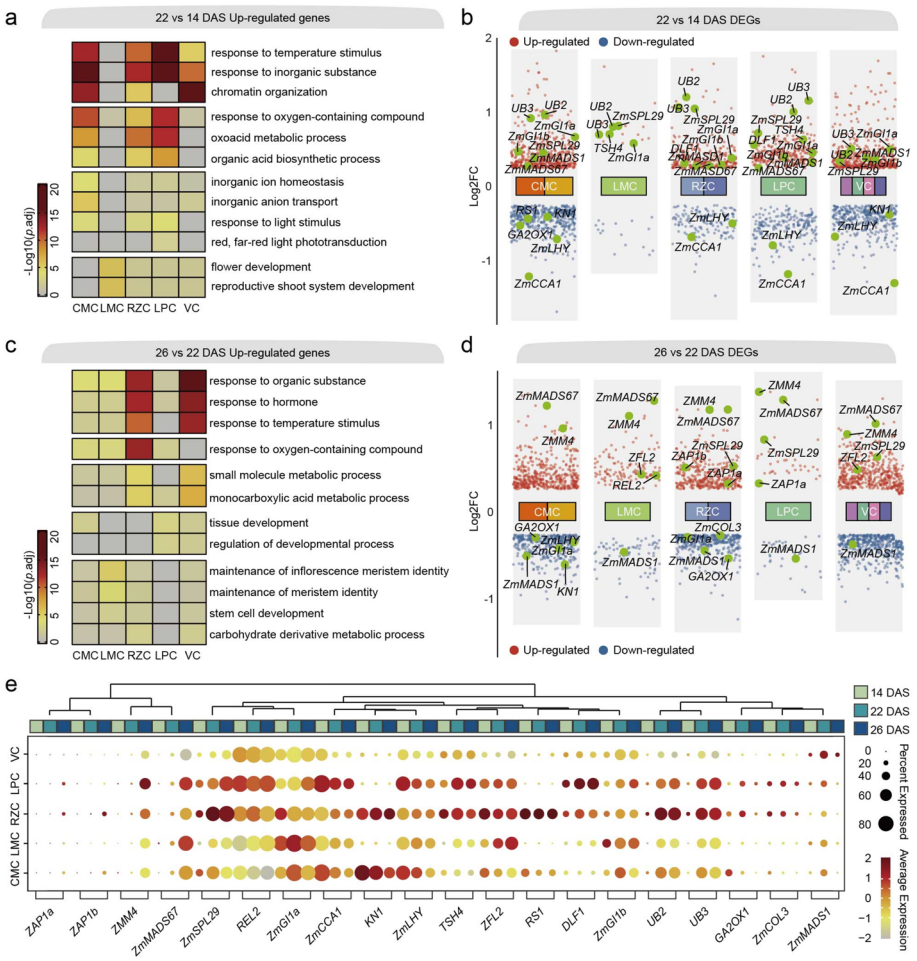

Fig. 4 Cell type-specific and shared molecular features during the maize floral transition. **a**, **c** Heatmaps showing top representative GO terms of up-regulated genes across five cell types between 22 vs 14 DAS (a) and 26 vs 22 DAS (c). **b**, **d** Differential expression analysis in five cell types between 22 vs 14 DAS (c) and 26 vs 22 DAS (d). DEGs were identified by adjusted *p* value < 0.01. Key regulatory genes are highlighted and labeled. **e** Expression patterns of 20 known floral transition and inflorescence regulators across five cell types and stages. Circle size indicates the percentage of cells expressing each gene, and color represents *Z*-score normalized expression level

domains serve as recognition sites for systemic florigen signals. In contrast, meristem maintenance genes *KN1* and *RS1*, as well as the gibberellin catabolic gene *GA2ox1*, were downregulated in CMC (Fig. 4b). This could create a permissive high-GA, low-KNOX environment for the reproductive transition.

Meanwhile, some DEGs exhibited broader cell type responses (Fig. 4e). For example, during the early floral transition (22 vs 14 DAS), we observed upregulation of the age-dependent *miR156*-targets, *SBP-box* transcription factors *UB2*, *UB3*, and *ZmSPL29* [28, 30], and downregulation of the circadian clock repressors *ZmLHY* and *ZmCCA1* [19, 20] across most of cell types (Fig. 4b). These observations suggest that the age-dependent acquisition of floral competency and resetting of the circadian oscillator occur ubiquitously rather than in specific cell types. Further, the floral integrator *ZmMADS1* (*SOC1* homolog) [61] showed a broad activation pattern in the RZC, LPC, CMC, and VC (Fig. 4b), in line with its role as an integrator merging the diverse floral induction signals in *Arabidopsis* [61]. Strikingly, the LMC had only 10 DEGs during the transition (Additional file 1: Fig. S12a), although its cell numbers increased dramatically, suggesting the LMC was likely not involved in the floral transition.

As the SAM progressed to reproductive stages (26 vs 22 DAS), the transcriptional program shifted from floral transition to the establishment of inflorescence identity. This phase was defined by the dramatic activation of the flower identity *MADS-box* genes *ZMM4* and *ZmMADS67* [27, 34] across all cell types, along with the universal downregulation of the early inductive factor *ZmMADS1* (Fig. 4d, e) [61]. Strikingly, the CMC, VC, and RZC were transcriptionally reprogrammed to express genes enriched in response and metabolic processes (Fig. 4c), presumably to support the energetic demands of rapid growth. The LMC displayed pronounced transcriptional changes (117 up-regulated DEGs) (Additional file 1: Fig. S12a) and enriched for stress responses and maintenance of meristem identity (Fig. 4d). This activation was associated with the floral identity gene *ZFL2* (*LEAFY* homolog) and the transcriptional corepressor *REL2* (Fig. 4d), representing the establishment of spikelet meristem indeterminacy and identity [62, 63]. In contrast, the LPCs showed fewer transcriptional changes (only 35 up-regulated DEGs) (Fig. 4d, Additional file 1: Fig. S12a), in line with the termination of leaf primordia formation after the floral transition. Collectively, these data characterize the maize floral transition as a highly coordinated process, where spatiotemporal compartmentalization allows for the organized integration of floral signals and the sequential execution of distinct transcriptional programs.

Distinct gene modules underpin meristem differentiation trajectories during the floral transition

In light of the continuous cell fate differentiation during the floral transition, we subsequently analyzed the differentiation trajectories among meristem-related cells (CMC, LMC, and RZC) using Monocle2 [64] to identify potential molecular signals in this process. This analysis resolved nine distinct cell states along a continuous developmental trajectory (Fig. 5a). State 8 was considered to be at the start of a trajectory, given that it was predominantly composed of cluster 3 (Fig. 5a, b), which contained high proportion (43%) of vegetative cells from 14 DAS (Fig. 3d). Following state 8, the trajectory bifurcated into two distinct branches. One branch composing state 7 exhibited a

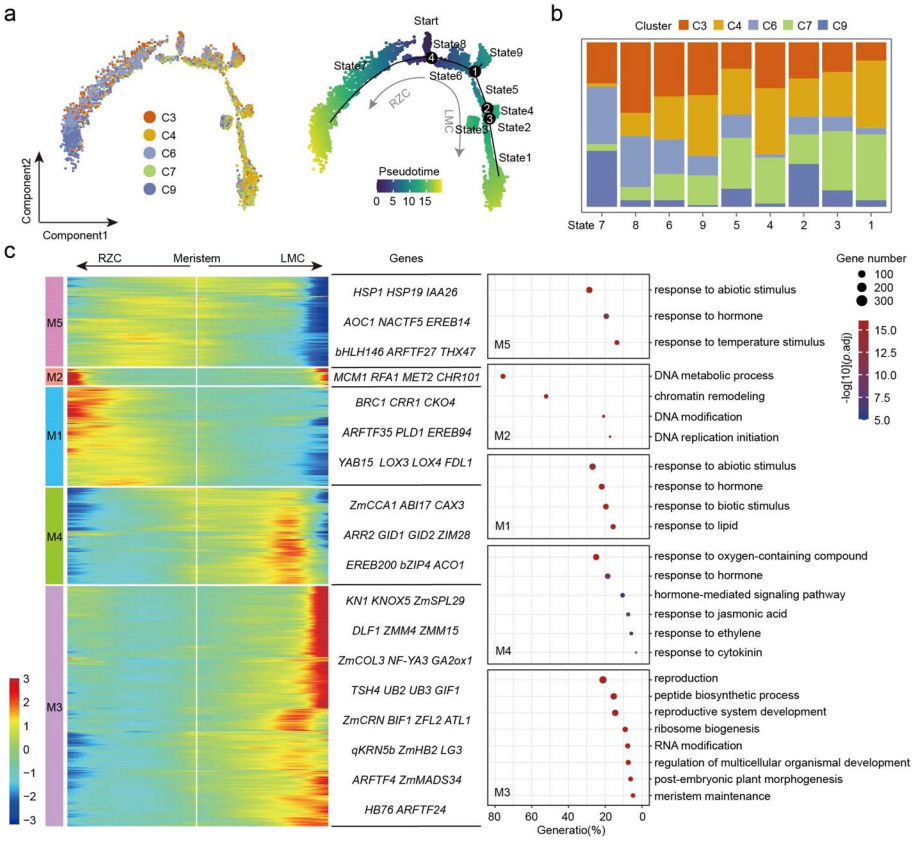

Fig. 5 Molecular features along meristem cell differentiation trajectory. **a** Differentiation trajectory of meristem-related cells (clusters 3, 4, 6, 7, 9). Colored dots represent cells from different cell clusters (left panel), and the corresponding pseudotime is shown on the right. **b** Cell percentages of different clusters in each pseudotime state. **c** Heatmap showing five modules of molecular drivers along the trajectory with selected representative genes and top enriched GO terms displayed on the right

progressive enrichment of rib zone cells (cluster 6, 9), while the other was characterized by an increased proportion of lateral meristem cells (cluster 7) and transition central meristem cells from DAS 22 and 26 (cluster 4) (Fig. 5a, b). This trajectory was validated by the unsupervised Palantir method (Additional file 1: Fig. S13a). Consistently, Palantir [65] pseudotime inference identified two major developmental branches, one corresponding to the RZC and the other to the LMC, with the root cell inferred automatically by the algorithm (Additional file 1: Fig. S13b). We next identified 3,688 highly variable genes along the trajectory and grouped them into five distinct gene modules (M1-M5) (Fig. 5c). Genes in module M5, predominantly expressed at the early phase of the trajectory, were enriched in responses to abiotic, temperature, and hormone stimuli, including heat shock protein genes *heat shock protein1* (*HSP1*) and *heat shock protein2* (*HSP2*) (Fig. 5c). At the distal end of the left trajectory branch, M1 and M2 genes were enriched in responses to diverse stimuli and DNA activities, respectively (Fig. 5c), likely associated with rib zone cell differentiation during floral induction. M4 genes were enriched at the middle of the right branch and associated with responses to hormones, especially jasmonic acid, ethylene, and cytokinin (Fig. 5c). Notably, M3 genes were highly expressed at the terminal end of the right branch and were enriched for processes of reproductive

development, as well as peptide biosynthesis and RNA modification (Fig. 5c). This module included several key floral transition genes *ZmSPL13/29*, *ZMM4*, and *DLF1* [26–28], and inflorescence meristem regulators *GRF-interacting Factor1* (*GIF1*), *UB2*, *UB3*, *TSH4*, and *BARREN INFLORESCENCE1* (*BIF1*) (Fig. 5c) [29, 30, 63, 66]. This result suggests that M3 genes represent potential regulators of the end of the floral transition and early inflorescence development. Together, the cell-differentiation trajectories revealed molecular features that are likely responsible for the differentiation of meristem-related cells during the floral transition, as well as inflorescence meristem establishment.

Identification of core floral transition regulators through co-expression network analysis

To uncover key regulators involved in the floral transition, we constructed a gene co-expression network (GCN) using the 5,856 genes with high variability across all cell types using hdWGCNA [67]. These genes were grouped into 18 distinct co-expression modules (M1-M18), and each comprised of 59 (M7) to 1,315 (M4) co-expressed genes (Additional file 1: Fig. S14a, b). These modules displayed distinct spatial expression patterns on the UMAP, often spanning multiple cell domains (Fig. 6a). For instance, module 5 was enriched in the central and lateral meristem regions, whereas module 4 showed relative enrichment in the rib meristem and leaf primordia (Fig. 6a). Such patterns suggest coordinated regulation across functionally distinct cell populations during the floral transition. To identify candidate regulators within each module, we calculated the intramodular connectivity and identified the top 10 hub genes for each module (Additional file 1: Fig. S14c), which were highlighted in the reconstructed GCN networks (Fig. 6b, c, Additional file 1: Fig. S15). Notably, the hub genes in module 3 included four benzoxazinoid (*BX*) biosynthesis genes and *SnRKII7*, both involved in abiotic stress responses and signal transduction [68, 69], indicating a potential role for this module in stress adaptation. Known floral transition-promoting genes *ZmSPL29*, *ZMM4*, and *ZMM15* [27, 28] were identified as hub genes in module 7 (Fig. 6b). Consistent with this, genes in module 7 were enriched in GO terms related to reproduction and shoot system development (Additional file 1: Fig. S16a), supporting their functional relevance to floral induction. Conversely, module 2 harbored *ZmLHY1* and *ZmCCA1*, which are central components of the circadian clock and act as repressors of flowering (Fig. 6c) [20, 70]. Genes in this module were highly enriched in primary metabolic processes (Additional file 1: Fig. S16b), suggesting metabolic processes mediate the effects of circadian clock on floral induction in maize.

To further examine the dynamic activity of these modules, we conducted differential module analysis across developmental stages. Module 7 showed the strongest upregulation from 14 to 22 DAS and also from 22 to 26 DAS, while module 2 exhibited a marked downregulation over the same periods (Fig. 6d, Additional file 1: Fig. S16c). These opposing trends mirror the functional distinction of the two modules and reinforce their potential positive and negative roles in the floral transition, respectively. Consistently, mutations in *ZmCCA1* and *ZmLHY1* in the negative module 2 lead to late flowering [20, 70]. For the positive module 7, we selected two hub genes, *UB2* and *UB3* previously implicated in inflorescence development [30], to investigate their roles in the floral transition. Both genes displayed progressively increased expression from 14 to 26 DAS in bulk RNA-seq and single-cell RNA-seq (Additional file 1: Fig. S1a, Fig. 4a). Our analysis

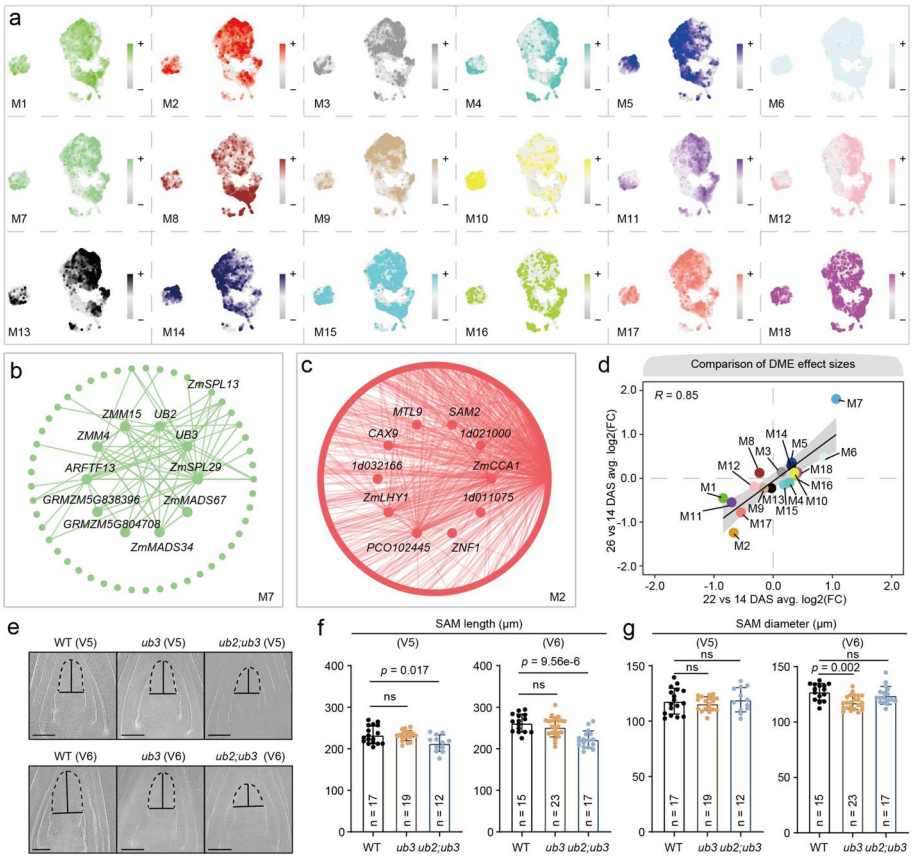

Fig. 6 Co-expression network analyses identify core floral transition regulators. **a** UMAP expression visualization of 18 gene co-expression modules identified by hdWGCNA. **b**, **c** hdWGCNA module network showing the top 10 hub genes in modules 7 (**b**) and 2 (**c**). **d** Comparison of effect size of cross-stage module differentials by DME testing. **e** Representative images of SAMs from WT, *ub3*, and *ub2;ub3* at V5 and V6 stages. Black lines indicate SAM regions for length and diameter measurements. Scale bars, 50 μm. **f**, **g** Quantification of SAM length (**f**) and diameter (**g**) in WT, *ub3*, and *ub2;ub3* plants at V5 and V6 stages. Statistical analyses were performed using two-tailed *t*-tests

of SAM size revealed that *ub2;ub3* double mutants had significant shorter SAMs at both V5 and V6 stages, however SAM width was not significantly altered (Fig. 6e-g). However, *ub3* single mutants showed no obvious change, presumably due to redundancy. Our results suggest that *UB2* and *UB3* promote the floral transition.

Discussion

The floral transition represents one of the most pivotal developmental switches in plants, where the shoot apical meristem (SAM) shifts from vegetative growth to reproductive identity. In maize, this transition not only determines flowering time and adaptation range but also fundamentally impacts yield-related traits [4, 5]. Despite the identification of major floral transition genes in maize (e.g., *ZCN8*, *DLF1*, *ZmRap2.7*) [13, 14, 26, 27, 46], the molecular basis of how SAM cells fine-control their identities during the transition has remained poorly understood. In this study, we constructed a high-resolution spatiotemporal transcriptome atlas of the maize SAM across the floral transition, and revealed that the transition is not a uniform event but a highly cell type coordinated and

phased orchestration involving the hierarchical transcriptional reprogramming and the precise execution of cell-type-specific regulatory modules.

Hierarchical transcriptional reprogramming and conserved modules underlie the maize floral transition

Our bulk transcriptome analysis across 14–28 DAS uncovered a continuous transcriptional trajectory, partitioning SAM development into three major phases: vegetative ($\leq$14 DAS), transitional (16–22 DAS), and post-transition ($\geq$26 DAS or early) in the B73 background. This phasing was marked by distinct gene clusters enriched in different biological processes, representing the hierarchical transcriptional reprogramming during the floral transition (Fig. 1). Notably, maize displays an early association with epigenetic remodeling at the onset of transition, reminiscent of the epigenetic repression of *FLC* which is required for flowering in *Arabidopsis* [44, 71]. Following epigenetic remodeling, the SAM activates the molecular modules enriched with environmental response genes, reflecting the integration of internal and external cues to trigger floral induction. This is associated with maize's broad adaptation to variable growth conditions under different photoperiods and temperatures [18, 21, 72]. The later stage (26–28 DAS) is characterized by robust induction of reproductive regulators (*RA2*, *VT2,* and *UB3*) [30, 31, 45], marking the commitment to inflorescence identity. The spatiotemporal transcriptome atlas of the maize SAM across the floral transition has been extensively characterized here.

Furthermore, our analysis uncovered a core regulatory module centered on *ZmMADS69-ZmRap2.7*, revealing how *MADS-* and *AP2*-family factors cooperate to gate floral transition outputs. *ZmMADS69* has been reported to promote flowering by repressing the flowering suppressor *ZmRap2.7* and concomitantly activating the florigen *ZCN8*, however it remains unclear whether the regulation is direct or indirect [47]. Here, we provide direct binding evidence for the ZmMADS69-ZmRap2.7 interaction, further validated by the mutant analysis (Fig. 2). Meanwhile, we have revealed that the floral identity gene *ZMM4* is a direct repression target of ZmRap2.7, suggesting a hierarchical regulatory module mediating the floral transition. *ZmMADS69*, with maximal expression in mature leaf, functions through the ZmRap2.7-ZCN8 regulatory module in the leaf [47]. Notably, our data suggests that the *ZmMADS69-ZmRap2.7* axis functions not only in leaf to promote florigen output, but also locally in the SAM to gate floral commitment. The dual roles of *AP2*-type flowering factors in both leaves and SAM have been reported in maize and *Arabidopsis* [36, 73]. In maize, the AP2 gene GL15 closely related to ZmRap2.7, directly binds and represses *ZMM4* in the SAM to induce flowering [36]. *GL15* could also directly reduce GA levels and delay flowering in leaves as well as in the SAM. In parallel, *Arabidopsis AP2* repression by the flowering integrator SOC1 (ortholog of ZmMADS1), together with the reciprocal repression of *SOC1* by AP2, contributes to synchronizing changes in meristem state, resulting in the floral transition [74]. Although this reciprocal repression between *ZmRap2.7* and *ZmMADS69* was not detected in our study, these studies have exposed the parallel functions of *MADS-AP2* modules in monocots and dicots.

Together, we have provided a full view of transcriptional features and dynamics of the maize SAM across the floral transition. Our mechanistic findings supported by the

genetic evidence greatly expand our understanding of the molecular control of the conserved regulation of this pivotal developmental process.

Spatially distinct regulatory domains integrate multiple signals to drive floral transition

Our scRNA-seq data analysis indicates that the maize floral transition is not driven by a uniform transcriptional switch, but instead emerges from the coordinated actions of spatially distinct cellular domains with highly specialized transcriptional programs. This spatial deployment is supported by domain-specific molecular changes, including the progressive downregulation of the meristem maintenance gene *KN1* in the central meristem (Fig. 4b, d), which may weaken the meristematic cells fate of the SAM [75]; reduced expression of the GA catabolic gene *GA2ox1* in the central meristem and rib zone (Fig. 4b, d), potentially elevating bioactive GA levels to promote meristem enlargement and rachis elongation [75–77]; and the selective activation of *ZFL2*, *TSH4*, and *REL2* in lateral meristem (Fig. 4b, d), consistent with their roles in floral identity, bract suppression, and meristem determinacy [29, 62, 78]. The rib zone and leaf primordia in maize likely act as primary sites for florigen signal perception, as indicated by strong activation of the florigen mediator *DLF1* (Fig. 4b, e) [34]. These locally perceived signals are likely subsequently integrated and propagated throughout the SAM by the flowering integrator *ZmMADS1* [61], which is broadly induced across all SAM domains (Fig. 4b, e). As development proceeds, the initially broad activation of *ZmMADS1* is followed by its universal downregulation, coinciding with the strong induction of the floral transition genes *ZMM4* and *ZmMADS67* (Fig. 4d, e). This dynamic parallel the *SOC1-AP1* transcriptional handoff in *Arabidopsis*, in which *SOC1* is transiently induced and subsequently repressed upon *AP1* activation [79]. In parallel, enrichment of chromatin organization processes in the CMC and RZC suggests that epigenetic remodeling contributes to the acquisition of reproductive competence in these domains, echoing the observations in *Arabidopsis* that chromatin-based reprogramming accompanies the vegetative-to-reproductive transition [80].

Although the floral transition is governed by a conserved core regulatory logic across angiosperms, its temporal dynamics and spatial organization probably varies among species. In *Arabidopsis*, this process is temporally compressed and executed within a relatively small SAM [6]. In rice, the transition unfolds over a longer developmental window, involving intermediate stages such as panicle meristem formation [81, 82]. Our data indicates that maize undergoes a markedly prolonged (16–22 DAS or longer) and spatially structured floral transition, in which regulatory signals are deployed across distinct domains with divergent functions. In addition, GO analysis suggests that temperature acts as a dominant environmental signal to trigger the floral transition. In *Arabidopsis* and rice, meristem transitions are sensitive to light signals, which may limit the adaption area of different rice varieties. In contrast, maize can be planted in broader regions with large day-length differences, and without striking effects on flowering time. The suggestion that maize flowering is more sensitive to temperature could inform strategies to manipulate the flowering time of maize. We recognize that our current three-stage sampling for scRNA-seq may miss transient molecular events; however, this approach was necessary to ensure sufficient biological material for high-quality library preparation,

and it provides a foundational framework for future studies with even finer temporal resolution.

Dual roles of *UB2/UB3* in coordinating floral transition and inflorescence architecture

Our single-cell transcriptomic analysis found that the SBP-box transcription factors *UB2* and *UB3* are activated at an early stage of floral induction (Fig. 4b). Functional analyses further support their promotive roles in facilitating SAM elongation during the transition phase (Fig. 6e-g). These findings extend the reported roles of *UB2/UB3* in inflorescence architecture by promoting lateral meristem formation while constraining inflorescence meristem (IM) activity [30]. Together, our results indicate that *UB2/UB3* possess dual functions, coordinating both floral induction and subsequent inflorescence development. Consistent with this view, co-expression network analysis places *UB2/UB3* within a regulatory module that includes key genes for floral transition and IM identity, such as *ZMM4*, *ZmMADS67*, *ZmSPL13*, and *ZmSPL29* (Fig. 6b). Notably, *ZmSPL13* and *ZmSPL29* directly activate miR172 and *ZCN8* in leaves, as well as *ZMM3* and *ZMM4* in the SAM, thereby linking age-dependent signaling to both systemic florigen production and local floral identity establishment [28]. These functions parallel the conserved miR156-SPL-miR172 cascade described in *Arabidopsis* and rice [83–85]. For example, *OsSPL14/IPA1*, regulated by miR156, simultaneously influences flowering time, tiller number, and panicle branching, illustrating how *SPL* activity integrates reproductive timing with inflorescence patterning in grasses [84, 85]. Taken together, these observations suggest that *UB2/UB3* regulate both floral transition and subsequent inflorescence development likely through a conserved miR156-SPL-miR172 regulatory mechanism, which needs further validation.

Conclusions

We generated a high-resolution spatiotemporal transcriptome atlas of the maize shoot apical meristem during the floral transition, revealing a hierarchical and multi-domain coordinated regulatory framework underlying this process. We identified a *ZmMADS69-ZmRap2.7-ZMM4* negative feed-forward loop that fine-tunes the timing of floral transition, together with a *UB2-UB3*-centered module that links floral induction with subsequent inflorescence development. Collectively, these findings provide mechanistic insights into how regulatory signals are spatially and temporally integrated to orchestrate floral transition in maize.

Methods

Plant materials and growth conditions

All sequencing experiments were conducted using the maize inbred line B73. Plants were grown in pots under greenhouse conditions for SAM collection. For bulk RNA-seq, SAMs were harvested at 14, 16, 18, 22, 26, and 28 days after sowing (DAS), corresponding to the V3-V7 developmental stages. For ATAC-seq, SAMs were collected at 14, 22, and 26 DAS. For scRNA-seq, SAMs with the two youngest leaf primordia attached were collected at 14, 22, and 26 DAS. For tsCUT&Tag, B73 plants were grown in an indoor plant incubator under continuous dark conditions to obtain etiolated leaves for protoplast extraction. The scRNA-seq experiment was performed with one biological

replicate, each consisting of approximately ~ 300 pooled SAMs, whereas all other sequencing assays were carried out with two biological replicates, each comprising ~ 25 SAMs. For mutant analyses, a *Mu* transposon insertion mutant of *ZmMADS69* in the W22 background and a CRISPR/Cas9 knockout mutant of *ZmRap2.7* in the B73 background were obtained from the National Maize Improvement Center of China, both of which have previously been reported to affect maize flowering time [47]. *Mu* transposon insertion mutants *ub2-mum1* and *ub3-mum3* were obtained from the Maize Genetics Cooperation Stock Center and backcrossed to B73 for three times; both mutants have been reported to affect inflorescence development [30]. For phenotyping, segregating seeds from all mutant lines were grown either in the field or in pots under greenhouse conditions, and SAM size was measured at the V5 and V6 stages.

Bulk RNA-seq library preparation

SAM samples at 14, 16, 18, 22, 26, and 28 DAS were flash-frozen with liquid nitrogen immediately after collection. Total RNA was extracted using the Direct-zol RNA Microprep Kit (Zymo Research). Sequencing libraries were constructed with the MGIEasy RNA Library Prep Kit according to the manufacturer's instructions.

ATAC-seq library preparation

ATAC-seq libraries were constructed following previously established protocol [86] with some modifications to accommodate the small size of maize SAMs. For each replicate, approximately 25 freshly dissected SAMs were digested in 15 μl protoplast lysis buffer [39] at the bottom of 1.5 ml tube for 2 h at room temperature in the dark with gentle shaking. Nuclei were released by adding 1 ml release buffer (1 × PBS, 1 × protease inhibitor, 0.3% Triton X-100) and gentle pipetting. Nuclei were then collected by centrifugation and resuspended in 20 μl 1 × TTBL buffer (Vazyme, TD501). Nuclei integrity and concentration were assessed by DAPI staining. Approximately 5,000 nuclei were subjected to Tn5 transposition (Vazyme, TD501) in the presence of 0.3% Triton X-100 at 37 °C for 30 min. Transposed DNA was immediately purified using Qiagen MinElute kits and amplified for 10–13 PCR cycles according to the manufacturer's instructions (VAHTS, TD501). Amplified DNA was size-selected using KAPA DNA Clean Beads (150–650 bp) to generate the final library, which was sequenced on an Illumina HiSeq X Ten platform (paired-end, 2 × 150 bp).

tsCUT&Tag libraries preparation

We conducted tsCUT&Tag assays following the reported protocol [87, 88]. In brief, full-length coding sequences of *ZmMADS69* and *ZmRap2.7* were cloned into the *PM999-GFP* vector, and plasmids were purified to transfection grade. Protoplasts were prepared from etiolated B73 seedlings grown in the dark and transfected with the GFP-tagged constructs using PEG-mediated transformation. After overnight incubation, protoplasts were processed using the Hyperactive In-Situ ChIP Library Prep Kit (Vazyme, Nanjing, China) according to the manufacturer's instructions. Chromatin was immunoprecipitated with anti-GFP antibody (1:100 dilution), and tagmented DNA fragments were PCR-amplified and size-selected to generate sequencing libraries. Libraries were subjected to paired-end sequencing (2 × 150 bp) on an Illumina NovaSeq 6000 platform.

scRNA-seq library preparation

scRNA-seq protoplasts were prepared as previously described [39, 41] with minor modifications. For each sample, approximately ~ 300 SAMs with two youngest leaf primordia were dissected and enzymatically digested in 50 µl protoplast lysis buffer at the bottom of 2 ml tube for 2 h at room temperature in the dark with gentle shaking to release protoplasts. After digestion, the reaction was stopped by dilution using 1.5 ml protoplast washing buffer (lysis buffer without enzyme) and filtered through 30-µm strainers to remove debris and large aggregates. The filtrate was then centrifuged at 300 g for 3 min at room temperature to collect protoplasts. Pellets were gently resuspended and washed twice with protoplast washing buffer under the same centrifugation conditions. After washing, a final filtration step was performed to remove cell aggregates and obtained a suspension of single, dissociated cells. Cell concentration and viability were assessed by fluorescein diacetate (FDA) staining using a hemocytometer. Only samples with $\geq$ 75% viable cells were used. Approximately 15,000 protoplasts were loaded into the BD Rhapsody™ Single-Cell Capture system (BD Biosciences) for scRNA-seq library construction according to the manufacturer's protocol. Libraries were sequenced on an Illumina NovaSeq 6000 platform with paired-end 150 bp reads.

Electrophoretic mobility shift assay

EMSA was performed using the EMSA Kit (LightShift Chemiluminescent EMSA Kit, Thermo Scientific) according to the user manual. Single-stranded DNA probes (40 to 50 bp) containing the "CArG" and "GCC-box" motifs within the 5' promoter of two potential targets, *ZmRap2.7* and *ZMM4*, were synthesized with or without 5' biotin labeling and dissolved to a final concentration of 10 µM. Annealing of forward and reverse probes into double-stranded DNA probes was carried out by heating at 95 °C for 5 min. For the binding reactions, approximately 1 µg of purified recombinant proteins (MBP, MBP-ZmMADS69, or MBP-ZmRap2.7) was incubated with the probes at room temperature for 20 min. The resulting protein-DNA complexes and free probes were separated by electrophoresis and detected via chemiluminescence. The specific sequences of all probes are provided in Additional file 2: Table S10.

Dual-luciferase reporter assay

The full-length coding sequences of *ZmMADS69* and *ZmRap2.7* were cloned into the *pGreenII 62-SK* vectors to generate effector constructs. 2-kb promoter fragments of *ZmRap2.7* and *ZMM4* were inserted into *pGreenII-0080-LUC* vectors, respectively, to create reporter constructs. Two effector-reporter combinations were tested: ZmMADS69 effector with ZmRap2.7 reporter, and ZmRap2.7 effector with ZMM4 reporter. The effector and reporter plasmids were co-transformed into protoplasts isolated from etiolated leaves of maize inbred line B73 following previous description [89]. After incubation, luciferase activity was quantified using the Promega Dual-Luciferase® Reporter Assay System (Madison, WI, USA) according to the manufacturer's instructions. Each assay was performed with at least three biological replicates.

qPCR analysis

Total RNA was extracted from SAM tissues of WT and mutant plants at V5 stage using Genstone Biotech RNA extraction kit (TR150). The RNA was reverse-transcribed with the Vazyme HiScript II One Step RT-PCR Kit (P611) to generate cDNA templates for qPCR. Quantitative PCR was conducted using Vazyme SYBR Green Mix (Q711) on a Bio-Rad CFX Connect real-time PCR system, and fluorescence signals were analyzed with Bio-Rad CFX Maestro software. ACTIN was used as the internal reference gene for normalization. Each assay included three biological replicates and experiment was repeated at least three times, yielding consistent results. Primer sequences for qPCR were documented in Additional file 2: Table S11.

RNA in situ hybridization

Shoot apices from different stage B73 plants were subjected to RNA in situ hybridization following established protocols [50]. For scRNA-seq marker gene probe preparation, T7 promoter sequence (5'-CATTAATACGACTCACTATAGGG-3') was incorporated into reverse primers to amplify gene-specific fragments from cDNA templates. Primer sequences are listed in Additional file 2: Table S12. Digoxigenin-labeled antisense probes were generated by *in vitro* transcription using a Roche transcription kit according to the manufacturer's instructions. Hybridization signals were imaged with a Nikon ECLIPSE DIC microscope.

SAM size measurement

Shoot apices at the V5 and V6 stages were dissected and longitudinally bisected through the shoot apex to generate thin sections. They were fixed overnight in ice-cold FAA solution (10% formaldehyde, 45% ethanol, and 5% acetic acid) and subsequently dehydrated through an ethanol series and cleared in 50% followed 100% methyl salicylate. Cleared shoot apices were imaged using a Nikon ECLIPSE DIC microscope. SAM measurement method was according to previous description [90]. Statistical analyses were performed in GraphPad Prism 8 software, and p values were calculated by two-tailed paired Student's t-tests.

Bulk RNA-seq analysis

Raw sequencing data quality was assessed using Trimmomatic (v.0.33) [91] with parameters "LEADING:20 TRAILING:20 SLIDINGWINDOW:4:15 MINLEN:20". Clean reads underwent alignment to the B73 AGPv4 reference genome via HISAT2 [92] under default settings. Uniquely mapped reads were extracted using SAMtools (v.1.9) [93] with filtering criteria "rmdup and mapq > 10". Transcript abundance quantification was performed through featureCounts (v.1.6.3) [94] using parameter "-p". Spatiotemporal clustering employed the LRT function in DESeq2 (v.1.26) [95], with subsequent sorting by k-means method. Principal component analysis visualization utilized DESeq2's "PlotPCA" function. Functional enrichment analysis was conducted via TBtools (v.1.120) [96].

tsCUT&Tag and ATAC-seq data analysis

Raw sequencing data quality control was performed using Trimmomatic [91] with parameters "LEADING:20 TRAILING:20 SLIDINGWINDOW:4:15 MINLEN:20". Clean

tsCUT&Tag and ATAC-seq reads were mapped to the maize genome (B73 AGPv4) via bowtie2 [97]. Post-alignment processing involved removing PCR duplicates and low-quality reads (mapping quality < 10) using samtools [93], followed by peak calling with MACS2 [98] under assay-specific parameters (tsCUT&Tag: used -s 150 -B –p5: ATAC-seq: –shift − 100 –extsize 200 –nomodel -B -SPMR). Replicate-concordant peaks were identified through the IDR statistical framework [99] at 5% IDR threshold. BEDtools [100] assigned OCRs to genes based on genomic proximity, defining regulatory regions as ± 3 kb from transcription start/termination sites. Transcription factor motif enrichment in accessible regions was analyzed using HOMER's "findMotifs.pl" function (v.4.10) [101] across differentially expressed gene sets. Genome browser tracks were visualized with pyGenomeTracks (v.3.6) [102].

scRNA-seq analysis, quality control and clustering

Clean UMI data were aligned to the maize genome using STAR mapping [103] with customized parameters to derive UMI counts per sample. All scRNA-seq preprocessing was executed in Seurat (v.4.3.0) [49]. Cellular metrics including detected total genes (nFeature_RNA), molecules (nCount_RNA), and mitochondrial/chloroplast genome mapping percentages (percent.mt/percent.pt) were quantified per sample. Quality control applied sequential filters: cells retaining 1,800–10,000 expressed genes and 2,800–50,000 UMIs; genes detected in at least 3 cells; exclusion of cells with percent. mt or percent.pt ≥ 10%; and doublet removal via DoubletFinder (v.2.0.3) [104]. Subsequently, scRNA-seq datasets from the three developmental time points were integrated using the Harmony algorithm to minimize batch effects. To further refine the data, we performed covariate regression during the "ScaleData" step, specifically regressing out technical and biological noise associated with protoplasting-induced genes and cell-cycle-related variation based on previously published marker sets [39, 40]. Cluster analysis entailed dimensionality reduction with "RunPCA", utilizing top 15 principal components for "FindNeighbors" and UMAP visualization. Cell clusters were defined by "FindClusters" (resolution = 1.0), with cluster-specific marker genes detected using "FindAllMarkers" (thresholds: p adj < 0.05, log2FC > 0.5, min.pct = 0.25). Stage-comparative DEGs in shoot apex cell types were computed via "FindMarkers", and functional enrichment analysis performed in TBtools [96].

Trajectory inference and pseudotime analysis

Pseudotime trajectories during the SAM floral transition were constructed with Monocle2 (v.2.18.0) [64]. Raw counts from clusters 3, 4, 6, 7, and 9 served as input. Genes meeting criteria (mean expression ≥ 0.1; dispersion empirical > dispersion fit value) were classified as high-variant genes (HVGs). Cell ordering along pseudotime was executed using HVGs and visualized in reduced dimensions via the DDRTree algorithm. Monocle's BEAM function identified branch-dependent genes (q value < 1e-4) andwere visualized by the "plot_genes_branched_heatmap" function. Gene clusters derived from heatmaps received functional annotation and GO term enrichment analysis using TBtools [96]. To assess the robustness of the developmental pathways identified by Monocle2 [64], we performed an independent trajectory analysis using Palantir [65]. First, a diffusion map was constructed from PCA projections (n_components = 5) using

the "palantir.utils.run_diffusion_maps" function. The developmental root cell was automatically designated using the "palantir.utils.early_cell" function. We then calculated the pseudotime and branching probabilities for the cells of clusters 3, 4, 6, 7 and 9, which were visualized using the "palantir.plot.plot_trajectories" function.

scRNA-seq co-expression analysis

To reveal the co-expression correlations between genes, a weighted gene co-expression network (WGCN) was created by the hdWGCNA (0.3.1) R package [67] using all cells. After setting up Seurat object for WGCNA, metacells were constructed with the following parameters: k = 25, assay = "RNA", max_shared = 10, min_cells = 100, slot = "data". Only cells within the same cell type in the same sample were pooled for metacell construction. "ConstructNetwork" function was used to construct co-expression network with a soft-power threshold of 5. We computed MEs for these modules using the hdWGCNA function "ModuleEigengenes", applying a "Harmony" correction to the Mes based on the sequencing batch. Next, we computed eigengene-based connectivity (kME) for each gene using the hdWGCNA function "ModuleConnectivity". Further, we identified differentially co-expression modules across the three stages through the hdWGCNA function "FindDMEs". ALL co-expression networks were visualized using the hdWGCNA function "ModuleNetworkPlot".

Supplementary Information

The online version contains supplementary material available at https://doi.org/10.1186/s13059-026-04033-x.

Additional file 1: Supplementary figures. Fig. S1. Overview of transcriptome dynamics. Fig. S2. Characterization of OCRs in three SAM stages during floral transition. Fig. S3. Expression patterns of TF family members showing stage-specific enrichment, including AP2, ARR-B, LBD, DOF, G2-like, and MADS-box TFs. Fig. S4. Characterization of ZmMADS69 and ZmRap2.7 tsCUT&Tag data. Fig. S5. Full scans of the EMSA gels shown in Fig. 2c and 2k. Fig. S6. Characterization of SAM single-cell RNA-seq datasets. Fig. S7. Expression UMAP plots of marker genes used for predicting and validating cluster identities. Fig. S8. Boxplots of cell identity scores calculated using the "AddModuleScore" function in Seurat based on known marker genes. Fig. S9. Expression patterns of flowering-related genes across clusters 3, 4, 6, and 7. Fig. S10. Quality assessment and validation of scRNA-seq data. Fig. S11. Validation of cell-type annotations using published reference data. Fig. S12. Identification and comparison of DEGs during floral transition. Fig. S13. Diffusion component analysis and pseudotime inference using Palantir. Fig. S14. Construction of gene co-expression networks based on single-cell transcriptomics. Fig. S15. Additional hdWGCNA module networks. Fig. S16. Differential module analysis across developmental stages.

Additional file 2: Supplementary tables. Table S1. Summary of data generated in this study. Table S2. Spatiotemporal RNA clusters of DEGs, related to Fig. 1c. Table S3. Merged open chromatin regions of three stages ATAC-seq data. Table S4. Transcriptional profiles of TF family genes during different developmental stages, including AP2, ARR-B, LBD, DOF, G2-like, and MADS-box TFs. Table S5. Consistent peaks obtained with the IDR statistical between the two biological replicates of ZmMADS69 tsCUT&Tag. Table S6. Consistent peaks obtained with the IDR statistical between the two biological replicates of ZmRap2.7 tsCUT&Tag. Table S7. Single-cell cluster marker genes. Table S8. Differentially expressed genes (DEGs) between 14 and 22 days after sowing (DAS) for five cell types. Table S9. Differentially expressed genes (DEGs) between 22 and 26 days after sowing (DAS) for five cell types. Table S10. Primer sequences of EMSA assay. Table S11. Primer sequences for qPCR assay. Table S12. Primer sequences of RNA in situ hybridization.

Acknowledgements

We thank Spatial FISH for scRNA-seq library construction, and the computations in this paper were run on the bioinformatics computing platform of the National Key Laboratory of Crop Genetic Improvement, Huazhong Agricultural University.

Peer review information

Wenjing She was the primary editor of this article and managed its editorial process and peer review in collaboration with the rest of the editorial team. The peer-review history is available in the online version of this article.

Authors' contributions

F.Y., L.D., and Y.S. conceived and designed the project. L.D., L.K., Z.L., Y.L., H.S., and Y.S. performed the experiments. L.D., and Y.S. analyzed data. L.D., Y.S., and F.Y. wrote the manuscript. F.T., and D.J. reviewed and edited the manuscript. The authors read and approved the final manuscript.

Funding
This work was supported by the National Natural Science Foundation of China (U22A20460 and 32301835), the Shenzhen Science and Technology Program (KCXFZ20240903093007010 and JCYJ20240813151013018) and by the National Science Foundation (IOS-2129189 to DJ).

Data availability
The data generated in this study have been deposited in the NCBI with the accession number "GSE309101" and "PRJNA1398575" [105, 106]. The published SAM + P6 scRNA-seq data used in this study was downloaded from the NCBI SRA (PRJNA637882) [107].

Declarations

Ethics approval and consent to participate
Not applicable.

Consent for publication
Not applicable.

Competing interests
The authors declare no competing interests.

Received: 1 October 2025 Accepted: 6 March 2026
Published online: 18 March 2026

References

1. Matsuoka Y, Vigouroux Y, Goodman MM, Sanchez GJ, Buckler E, Doebley J. A single domestication for maize shown by multilocus microsatellite genotyping. Proc Natl Acad Sci U S A. 2002;99:6080–4.
2. Piperno DR, Ranere AJ, Holst I, Iriarte J, Dickau R. Starch grain and phytolith evidence for early ninth millennium B.P. maize from the Central Balsas River Valley, Mexico. Proc Natl Acad Sci U S A. 2009;106:5019–24.
3. Kuleshov NN. World's diversity of phenotypes of maize1. Agron J. 1933;25:688–700.
4. Colasanti J, Muszynski M. The Maize Floral Transition. In: Bennetzen JL, Hake SC, editors. Handbook of maize: its biology. New York: Springer; 2009. p. 41–55.
5. Irish EE, Nelson TM. Identification of multiple stages in the conversion of maize meristems from vegetative to floral development. Development. 1991;112:891–8.
6. Andrés F, Coupland G. The genetic basis of flowering responses to seasonal cues. Nat Rev Genet. 2012;13:627–39.
7. Zeevaart JAD. Physiology of flower formation. Annu Rev Plant Physiol Plant Mol Biol. 1976;27:321–48.
8. Corbesier L, Vincent C, Jang S, Fornara F, Fan Q, Searle I, et al. FT protein movement contributes to long-distance signaling in floral induction of *Arabidopsis*. Science. 2007;316:1030–3.
9. Abe M, Kobayashi Y, Yamamoto S, Daimon Y, Yamaguchi A, Ikeda Y, et al. FD, a bZIP protein mediating signals from the floral pathway integrator FT at the shoot apex. Science. 2005;309:1052–6.
10. Wigge PA, Kim MC, Jaeger KE, Busch W, Schmid M, Lohmann JU, et al. Integration of spatial and temporal information during floral induction in *Arabidopsis*. Science. 2005;309:1056–9.
11. Jaeger KE, Wigge PA. FT protein acts as a long-range signal in *Arabidopsis*. Curr Biol. 2007;17:1050–4.
12. Mathieu J, Warthmann N, Küttner F, Schmid M. Export of FT protein from phloem companion cells is sufficient for floral induction in *Arabidopsis*. Curr Biol. 2007;17:1055–60.
13. Lazakis CM, Coneva V, Colasanti J. *ZCN8* encodes a potential orthologue of *Arabidopsis* FT florigen that integrates both endogenous and photoperiod flowering signals in maize. J Exp Bot. 2011;62:4833–42.
14. Meng X, Muszynski MG, Danilevskaya ON. The *FT*-like *ZCN8* gene functions as a floral activator and is involved in photoperiod sensitivity in maize. Plant Cell. 2011;23:942–60.
15. Dong Z, Danilevskaya O, Abadie T, Messina C, Coles N, Cooper M. A gene regulatory network model for floral transition of the shoot apex in maize and its dynamic modeling. PLoS One. 2012;7:e43450.
16. Sheehan MJ, Kennedy LM, Costich DE, Brutnell TP. Subfunctionalization of *PhyB1* and *PhyB2* in the control of seedling and mature plant traits in maize. Plant J. 2007;49:338–53.
17. Li Q, Wu G, Zhao Y, Wang B, Zhao B, Kong D, et al. CRISPR/Cas9-mediated knockout and overexpression studies reveal a role of maize *phytochrome C* in regulating flowering time and plant height. Plant Biotechnol J. 2020;18:2520–32.
18. Zhao Y, Zhao B, Wu G, Ma X, Wang B, Kong D, et al. Creation of two hyperactive variants of *phytochrome B1* for attenuating shade avoidance syndrome in maize. J Integr Agric. 2022;21:1253–65.
19. Chardon F, Virlon B, Moreau L, Falque M, Joets J, Decousset L, et al. Genetic architecture of flowering time in maize as inferred from quantitative trait loci meta-analysis and synteny conservation with the rice genome. Genetics. 2004;168:2169–85.
20. Wang X, Wu L, Zhang S, Wu L, Ku L, Wei X, et al. Robust expression and association of *ZmCCA1* with circadian rhythms in maize. Plant Cell Rep. 2011;30:1261–72.
21. Hung H, Shannon LM, Tian F, Bradbury PJ, Chen C, Flint-Garcia SA, et al. *ZmCCT* and the genetic basis of day-length adaptation underlying the postdomestication spread of maize. Proc Natl Acad Sci U S A. 2012;109:E1913-1921.
22. Huang C, Sun H, Xu D, Chen Q, Liang Y, Wang X, et al. *ZmCCT9* enhances maize adaptation to higher latitudes. Proc Natl Acad Sci U S A. 2018;115:E334–41.

23. Stephenson E, Estrada S, Meng X, Ourada J, Muszynski MG, Habben JE, et al. Over-expression of the photoperiod response regulator *ZmCCT10* modifies plant architecture, flowering time and inflorescence morphology in maize. PLoS One. 2019;14:e0203728.
24. Miller TA, Muslin EH, Dorweiler JE. A maize *CONSTANS*-like gene, *conz1*, exhibits distinct diurnal expression patterns in varied photoperiods. Planta. 2008;227:1377–88.
25. Heuer S, Hansen S, Bantin J, Brettschneider R, Kranz E, Lörz H, et al. The maize MADS box gene *ZmMADS3* affects node number and spikelet development and is co-expressed with *ZmMADS1* during flower development, in egg cells, and early embryogenesis. Plant Physiol. 2001;127:33–45.
26. Muszynski MG, Dam T, Li B, Shirbroun DM, Hou Z, Bruggemann E, et al. *delayed flowering1* encodes a basic leucine zipper protein that mediates floral inductive signals at the shoot apex in maize. Plant Physiol. 2006;142:1523–36.
27. Danilevskaya ON, Meng X, Selinger DA, Deschamps S, Hermon P, Vansant G, et al. Involvement of the *MADS-box* gene *ZMM4* in floral induction and inflorescence development in maize. Plant Physiol. 2008;147:2054–69.
28. Yang J, Wei H, Hou M, Chen L, Zou T, Ding H, et al. *ZmSPL13* and *ZmSPL29* act together to promote vegetative and reproductive transition in maize. New Phytol. 2023;239:1505–20.
29. Chuck GS, Whipple C, Jackson D, Hake S. The maize SBP-box transcription factor encoded by *tasselsheath4* regulates bract development and the establishment of meristem boundaries. Development. 2010;137:1243–50.
30. Chuck GS, Brown PJ, Meeley R, Hake S. Maize SBP-box transcription factors *unbranched2* and *unbranched3* affect yield traits by regulating the rate of lateral primordia initiation. Proc Natl Acad Sci USA. 2014;111:18775–80.
31. Bortiri E, Chuck G, Vollbrecht E, Rocheford T, Martienssen R, Hake S. Ramosa2 encodes a LATERAL ORGAN BOUNDARY domain protein that determines the fate of stem cells in branch meristems of maize. Plant Cell. 2006;18:574–85.
32. Satoh-Nagasawa N, Nagasawa N, Malcomber S, Sakai H, Jackson D. A trehalose metabolic enzyme controls inflorescence architecture in maize. Nature. 2006;441:227–30.
33. Vollbrecht E, Springer PS, Goh L, Buckler ES, Martienssen R. Architecture of floral branch systems in maize and related grasses. Nature. 2005;436:1119–26.
34. Sun H, Wang C, Chen X, Liu H, Huang Y, Li S, et al. Dlf1 promotes floral transition by directly activating *ZmMADS4* and *ZmMADS67* in the maize shoot apex. New Phytol. 2020;228:1386–400.
35. Teotia S, Tang G. To bloom or not to bloom: role of microRNAs in plant flowering. Mol Plant. 2015;8:359–77.
36. Yang J, Xu G, Zhang M, Xue W, Wu J, Li Y, et al. Dual role of *Glossy15* in regulating flowering by modulating gibberellins and floral organ gene expression in maize. New Phytol. 2025;248:2143–59.
37. Zhang T, Xu Z, Shang G, Wang J. A single-cell RNA sequencing profiles the developmental landscape of *Arabidopsis* root. Mol Plant. 2019;12:648–60.
38. Zhang T, Chen Y, Wang J-W. A single-cell analysis of the *Arabidopsis* vegetative shoot apex. Dev Cell. 2021;56:1056–74.
39. Satterlee JW, Strable J, Scanlon MJ. Plant stem-cell organization and differentiation at single-cell resolution. Proc Natl Acad Sci U S A. 2020;117:33689–99.
40. Xu X, Crow M, Rice BR, Li F, Harris B, Liu L, et al. Single-cell RNA sequencing of developing maize ears facilitates functional analysis and trait candidate gene discovery. Dev Cell. 2021;56:557–68.
41. Sun Y, Dong L, Kang L, Zhong W, Jackson D, Yang F. Progressive meristem and single-cell transcriptomes reveal the regulatory mechanisms underlying maize inflorescence development and sex differentiation. Mol Plant. 2024;17:1019–37.
42. Strable J, Wallace JG, Unger-Wallace E, Briggs S, Bradbury PJ, Buckler ES, et al. Maize *YABBY* genes *drooping leaf1* and *drooping leaf2* regulate plant architecture. Plant Cell. 2017;29:1622–41.
43. Liu L, Gallagher J, Arevalo ED, Chen R, Skopelitis T, Wu Q, et al. Enhancing grain-yield-related traits by CRISPR-Cas9 promoter editing of maize *CLE* genes. Nat Plants. 2021;7:287–94.
44. Ji X, Liu W, Zhang F, Su Y, Ding Y, Li H. H3K36me3 and H2A.Z coordinately modulate flowering time in *Arabidopsis*. J Genet Genomics. 2024;51:1135–8.
45. Phillips KA, Skirpan AL, Liu X, Christensen A, Slewinski TL, Hudson C, et al. Vanishing tassel2 encodes a grass-specific tryptophan aminotransferase required for vegetative and reproductive development in maize. Plant Cell. 2011;23:550–66.
46. Salvi S, Sponza G, Morgante M, Tomes D, Niu X, Fengler KA, et al. Conserved noncoding genomic sequences associated with a flowering-time quantitative trait locus in maize. Proc Natl Acad Sci U S A. 2007;104:11376–81.
47. Liang Y, Liu Q, Wang X, Huang C, Xu G, Hey S, et al. *ZmMADS69* functions as a flowering activator through the *ZmRap2.7-ZCN8* regulatory module and contributes to maize flowering time adaptation. New Phytol. 2019;221:2335–47.
48. Li Z, Gao F, Liu Y, Abou-Elwafa Sf, Qi J, Pan H, et al. *ZmGI2* regulates flowering time through multiple flower development pathways in maize. Plant Sci. 2023;332.
49. Stuart T, Butler A, Hoffman P, Hafemeister C, Papalexi E, Mauck WM, et al. Comprehensive integration of single-cell data. Cell. 2019;177:1888–902.
50. Jackson D, Veit B, Hake S. Expression of maize *KNOTTED1* related homeobox genes in the shoot apical meristem predicts patterns of morphogenesis in the vegetative shoot. Development. 1994;120:405–13.
51. Cao Y, Ma J, Han S, Hou M, Wei X, Zhang X, et al. Single-cell RNA sequencing profiles reveal cell type-specific transcriptional regulation networks conditioning fungal invasion in maize roots. Plant Biotechnol J. 2023;21:1839–59.
52. Guo Y, Chen X, Li J, Wang Q, Zhang S, Liu N, et al. Single-cell RNA sequencing reveals a high-resolution cell atlas of petals in *Prunus mume* at different flowering development stages. Hortic Res. 2024;11:uhae189.
53. Wang T, Wang F, Deng S, Wang K, Feng D, Xu F, et al. Single-cell transcriptomes reveal spatiotemporal heat stress response in maize roots. Nat Commun. 2025;16:177.
54. Ma L, Zhang N, Liu P, Liang Y, Li R, Yuan G, et al. Single-cell RNA sequencing reveals a key regulator *ZmEREB14* affecting shoot apex development and yield formation in maize. Plant Biotechnol J. 2025;23:766–79.
55. Zhang L, He C, Lai Y, Wang Y, Kang L, Liu A, et al. Asymmetric gene expression and cell-type-specific regulatory networks in the root of bread wheat revealed by single-cell multiomics analysis. Genome Biol. 2023;24:65.

56. Liu Q, Liang Z, Feng D, Jiang S, Wang Y, Du Z, et al. Transcriptional landscape of rice roots at the single-cell resolution. Mol Plant. 2021;14:384–94.
57. Kang M, Choi Y, Kim H, Kim S-G. Single-cell RNA-sequencing of *Nicotiana attenuata* corolla cells reveals the biosynthetic pathway of a floral scent. New Phytol. 2022;234:527–44.
58. Liew LC, You Y, Auroux L, Oliva M, Peirats-Llobet M, Ng S, et al. Establishment of single-cell transcriptional states during seed germination. Nat Plants. 2024;10:1418–34.
59. Li P, Liu Q, Wei Y, Xing C, Xu Z, Ding F, et al. Transcriptional landscape of cotton roots in response to salt stress at single-cell resolution. Plant Commun. 2023;5:100740.
60. Li X, Zhang X, Gao S. Single-cell RNA sequencing reveals the landscape of maize root tips and assists in identification of cell type-specific nitrate-response genes. Crop J. 2022;10:1589–600.
61. Alter P, Bircheneder S, Zhou L-Z, Schlüter U, Gahrtz M, Sonnewald U, et al. Flowering time-regulated genes in maize include the transcription factor *ZmMADS1*. Plant Physiol. 2016;172:389–404.
62. Bomblies K, Wang R-L, Ambrose BA, Schmidt RJ, Meeley RB, Doebley J. Duplicate *FLORICAULA/LEAFY* homologs *zfl1* and *zfl2* control inflorescence architecture and flower patterning in maize. Development. 2003;130:2385–95.
63. Galli M, Liu Q, Moss BL, Malcomber S, Li W, Gaines C, et al. Auxin signaling modules regulate maize inflorescence architecture. Proc Natl Acad Sci U S A. 2015;112:13372–7.
64. Qiu X, Hill A, Packer J, Lin D, Ma Y-A, Trapnell C. Single-cell mRNA quantification and differential analysis with Census. Nat Methods. 2017;14:309–15.
65. Setty M, Kiseliovas V, Levine J, Gayoso A, Mazutis L, Pe'er D. Characterization of cell fate probabilities in single-cell data with Palantir. Nat Biotechnol. 2019;37:451–60.
66. Zhang D, Sun W, Singh R, Zheng Y, Cao Z, Li M, et al. *GRF-interacting factor1* regulates shoot architecture and meristem determinacy in maize. Plant Cell. 2018;30:360–74.
67. Morabito S, Reese F, Rahimzadeh N, Miyoshi E, Swarup V. hdWGCNA identifies co-expression networks in high-dimensional transcriptomics data. Cell Rep Methods. 2023;3:100498.
68. Zhao X, Shi Z, He F, Niu Y, Qi G, Sun S, et al. Benzoxazinoids biosynthetic gene cluster identification and expression analysis in maize under biotic and abiotic stresses. Int J Mol Sci. 2024;25:7460.
69. Jiang S, Sun Z, Feng Z, Qi Y, Chen H, Wang Y, et al. *ZmCIPK33* and *ZmSnRK2.10* mutually reinforce the abscisic acid signaling pathway for combating drought stress in maize. J Integr Plant Biol. 2025;67:1787–804.
70. Hayes KR, Beatty M, Meng X, Simmons CR, Habben JE, Danilevskaya ON. Maize global transcriptomics reveals pervasive leaf diurnal rhythms but rhythms in developing ears are largely limited to the core oscillator. PLoS One. 2010;5:e12887.
71. Berry S, Dean C. Environmental perception and epigenetic memory: mechanistic insight through *FLC*. Plant J. 2015;83:133–48.
72. Li Y, Li C, Bradbury PJ, Liu X, Lu F, Romay CM, et al. Identification of genetic variants associated with maize flowering time using an extremely large multi-genetic background population. Plant J. 2016;86:391–402.
73. Yant L, Mathieu J, Dinh TT, Ott F, Lanz C, Wollmann H, et al. Orchestration of the floral transition and floral development in *Arabidopsis* by the bifunctional transcription factor *APETALA2*. Plant Cell. 2010;22:2156–70.
74. de Bertran Garcia Olalla E, Cerise M, Rodríguez-Maroto G, Casanova-Ferrer P, Vayssières A, Severing E, et al. Coordination of shoot apical meristem shape and identity by *APETALA2* during floral transition in *Arabidopsis*. Nat Commun. 2024;15:6930.
75. Bolduc N, Hake S. The maize transcription factor *KNOTTED1* directly regulates the gibberellin catabolism gene *ga2ox1*. Plant Cell. 2009;21:1647–58.
76. Kinoshita A, Vayssières A, Richter R, Sang Q, Roggen A, van Driel AD, et al. Regulation of shoot meristem shape by photoperiodic signaling and phytohormones during floral induction of *Arabidopsis*. Elife. 2020;9:e60661.
77. Sakamoto T, Kobayashi M, Itoh H, Tagiri A, Kayano T, Tanaka H, et al. Expression of a gibberellin 2-oxidase gene around the shoot apex is related to phase transition in rice. Plant Physiol. 2001;125:1508–16.
78. Gallavotti A, Long JA, Stanfield S, Yang X, Jackson D, Vollbrecht E, et al. The control of axillary meristem fate in the maize *ramosa* pathway. Development. 2010;137:2849–56.
79. Liu C, Zhou J, Bracha-Drori K, Yalovsky S, Ito T, Yu H. Specification of *Arabidopsis* floral meristem identity by repression of flowering time genes. Development. 2007;134:1901–10.
80. He Y. Chromatin regulation of flowering. Trends Plant Sci. 2012;17:556–62.
81. Itoh J, Nonomura K, Ikeda K, Yamaki S, Inukai Y, Yamagishi H, et al. Rice plant development: from zygote to spikelet. Plant Cell Physiol. 2005;46:23–47.
82. Tsuji H, Taoka K, Shimamoto K. Regulation of flowering in rice: two florigen genes, a complex gene network, and natural variation. Curr Opin Plant Biol. 2011;14:45–52.
83. Wu G, Park MY, Conway SR, Wang J-W, Weigel D, Poethig RS. The sequential action of *miR156* and *miR172* regulates developmental timing in *Arabidopsis*. Cell. 2009;138:750–9.
84. Jiao Y, Wang Y, Xue D, Wang J, Yan M, Liu G, et al. Regulation of *OsSPL14* by *OsmiR156* defines ideal plant architecture in rice. Nat Genet. 2010;42:541–4.
85. Miura K, Ikeda M, Matsubara A, Song X, Ito M, Asano K, et al. *OsSPL14* promotes panicle branching and higher grain productivity in rice. Nat Genet. 2010;42:545–9.
86. Sun Y, Dong L, Zhang Y, Lin D, Xu W, Ke C, et al. 3D genome architecture coordinates trans and cis regulation of differentially expressed ear and tassel genes in maize. Genome Biol. 2020;21:143.
87. Dong L, Shi Y, Li P, Zhong S, Sun Y, Yang F. Constructing the maize inflorescence regulatory network by using efficient tsCUT&tag assay. Crop J. 2023;11:951–6.
88. Wu L, Luo Z, Shi Y, Jiang Y, Li R, Miao X, et al. A cost-effective tsCUT&Tag method for profiling transcription factor binding landscape. J Integr Plant Biol. 2022;64:2033–8.
89. Yoo S, Cho Y, Sheen J. *Arabidopsis* mesophyll protoplasts: a versatile cell system for transient gene expression analysis. Nat Protoc. 2007;2:1565–72.
90. Leiboff S, Li X, Hu H-C, Todt N, Yang J, Li X, et al. Genetic control of morphometric diversity in the maize shoot apical meristem. Nat Commun. 2015;6:8974.

91. Bolger AM, Lohse M, Usadel B. Trimmomatic: a flexible trimmer for Illumina sequence data. Bioinformatics. 2014;30:2114–20.
92. Kim D, Langmead B, Salzberg SL. Hisat: a fast spliced aligner with low memory requirements. Nat Methods. 2015;12:357–60.
93. Li H, Handsaker B, Wysoker A, Fennell T, Ruan J, Homer N, et al. The sequence alignment/map format and SAMtools. Bioinformatics. 2009;25:2078–9.
94. Liao Y, Smyth GK, Shi W. Featurecounts: an efficient general purpose program for assigning sequence reads to genomic features. Bioinformatics. 2014;30:923–30.
95. Love MI, Huber W, Anders S. Moderated estimation of fold change and dispersion for RNA-seq data with DESeq2. Genome Biol. 2014;15:550.
96. Chen C, Chen H, Zhang Y, Thomas HR, Frank MH, He Y, et al. Tbtools: an integrative toolkit developed for interactive analyses of big biological data. Mol Plant. 2020;13:1194–202.
97. Langmead B, Salzberg SL. Fast gapped-read alignment with Bowtie 2. Nat Methods. 2012;9:357–9.
98. Zhang Y, Liu T, Meyer CA, Eeckhoute J, Johnson DS, Bernstein BE, et al. Model-based analysis of ChIP-Seq (MACS). Genome Biol. 2008;9:R137.
99. Li Q, Brown JB, Huang H, Bickel PJ. Measuring reproducibility of high-throughput experiments. Ann Appl Stat. 2011;5:1752–79.
100. Ar Q, Im H. Bedtools: a flexible suite of utilities for comparing genomic features. Bioinformatics. 2010;26:841–2.
101. Heinz S, Benner C, Spann N, Bertolino E, Lin YC, Laslo P, et al. Simple combinations of lineage-determining transcription factors prime cis-regulatory elements required for macrophage and B cell identities. Mol Cell. 2010;38:576–89.
102. Ramírez F, Bhardwaj V, Arrigoni L, Lam KC, Grüning BA, Villaveces J, et al. High-resolution TADs reveal DNA sequences underlying genome organization in flies. Nat Commun. 2018;9:189.
103. Dobin A, Davis CA, Schlesinger F, Drenkow J, Zaleski C, Jha S, et al. STAR: ultrafast universal RNA-seq aligner. Bioinformatics. 2013;29:15–21.
104. McGinnis CS, Murrow LM, Gartner ZJ. Doubletfinder: doublet detection in single-cell RNA sequencing data using artificial nearest neighbors. Cell Syst. 2019;8:329–37.
105. Dong L, Sun Y, Kang L, Li Z, Liang Y, Sheng H, Tian F, Jackson D, Yang F. Dynamic and cell-type specific transcriptional reprogramming underlies the floral transition in the maize shoot apical meristem. Bulk RNA-seq, ATAC-seq, tsCUT&Tag and scRNA-seq datasets. 2026. NCBI. https://www.ncbi.nlm.nih.gov/geo/query/acc.cgi?acc=GSE309101.
106. Dong L, Sun Y, Kang L, Li Z, Liang Y, Sheng H, Tian F, Jackson D, Yang F. Dynamic and cell-type specific transcriptional reprogramming underlies the floral transition in the maize shoot apical meristem. Bulk RNA-seq datasets. 2026. NCBI. https://www.ncbi.nlm.nih.gov/sra/?term=PRJNA1398575.
107. Satterlee JW, Strable J, Scanlon MJ. Plant stem-cell organization and differentiation at single-cell resolution. scRNA-seq datasets. 2020. NCBI. https://www.ncbi.nlm.nih.gov/sra?linkname=bioproject_sra_all&from_uid=637882.

Publisher's Note